Journal of Sound and Vibration 329 (2010) 1636–1652

Contents lists available at ScienceDirect

Journal of Sound and Vibration

journal homepage: www.elsevier.com/locate/jsvi

Effective suppression of pneumatic vibration isolators by using input–output linearization and time delay control

Pyung-hun Chang, Dong Ki Han *, Yun-ho Shin, Kwang-joon Kim

Robot Control Laboratory and Vibration Engineering Laboratory, Department of Mechanical Engineering, KAIST, Daejeon 305-701, South Korea

ARTICLE INFO

Article history:
Received 29 October 2009
Accepted 2 December 2009
Handling Editor: C.L. Morfey
Available online 13 January 2010

ABSTRACT

This paper presents a new state space representation of pneumatic vibration isolators (PVIs) and a design of a robust control, Time Delay Control (TDC), based on it. The new state space model, derived by using the input–output linearization method, is of the phase variable form with the air mass-flow as the control input. This model offers a framework that enables simultaneous suppression of both seismic vibration and direct disturbance (or payload disturbance) with an accelerometer only. Based on this model, TDC is designed and verified with experiments on a single chamber PVI with an accelerometer only. In the experiment, the PVI with TDC successfully suppresses seismic vibration and direct disturbance, both individually and simultaneously. Faced with seismic vibration, the transmissibility of the PVI with TDC has virtually no resonance peak at low frequency; under direct disturbance, the former achieves a 68 percent reduction in settling time of the latter. The final analysis of experimental result shows that TDC effectively estimates the modeling error along with other uncertainties and cancels them, while achieving desired closed-loop dynamics.

1. Introduction

The pneumatic vibration isolator (PVI) has found many applications in industry, thanks to its superior vibration isolation performance in the frequency range above the resonance.

There are two kinds of the mathematical model of the PVI: the one is represented in terms of equivalent elements of the payload, spring, and damper [1,2]; and the other is derived from inertial dynamics and first principles of thermodynamics [3]. For the sake of convenience, the former is termed in this article as the *mass-spring-damper* (*MSD*) *model*, and the latter the *physical model*.[1] The two models have completely different sets of state variables and control inputs, which are summarized in Table 1.

Based on the two models, two different lines of active controls have been proposed to improve the performance of the PVI as the following.

In the line based on the MSD model, in order to enhance the performance of a PVI under seismic vibration of the VC-C class [4], Shin and Kim [5,6] has adopted TDC with a promising result. Besides seismic vibration, An et al. [7] attempted to suppress direct disturbance by using a PID (Proportional-Integral-Derivative), with a result of about 65 percent improvement of the settling time of the payload. As an attempt to suppress *both* seismic vibration and direct disturbance, there was a research work by Kato and Kawashima [8,9] using PID control. The simultaneous suppression is a natural consequence, for the MSD model has the controllability canonical form with the two disturbances being directly controllable with its input [6,8,9].

* Corresponding author. Tel.: +82 42 350 3266; fax: +82 42 350 5226.
E-mail addresses: dkhan@mecha.kaist.ac.kr, cool-@kaist.ac.kr (D. Ki Han).

[1] The term 'physical model' has been adopted from [1].

0022-460X/$ - see front matter © 2009 Elsevier Ltd. All rights reserved.
doi:10.1016/j.jsv.2009.12.003

Table 1
Characteristics of two models.

	The mass-spring-damper model	The physical model
Important variables	The displacement of the payload The velocity of the payload	The velocity of the payload The pressure of the chamber
Control input	The pressure of the chamber	The air mass-flow to the chamber

As an active control based on the physical model, on the other hand, Chen and Shih used optimal control to enhance the robustness against seismic vibrations [10]. Thanks to the model characteristics, the control requires only an accelerometer, not wanting other sensors for pressure or for mass flow. The negative aspect of the model characteristics is that any control based on it is incapable of simultaneous suppression. In other words, the control input cannot affect both of seismic vibration and direct disturbance, and thus any active control based on the physical model is inherently unable to suppress both seismic vibration and direct disturbance simultaneously.

For the reasons mentioned above, we have taken a direction to derive a *new state space representation* that enables simultaneous suppression with only the accelerometer. The new state space model has been derived through the input–output linearization [11,12] of the physical model—the procedure and the result will be detailed in Section 2.

In addition to which model to select, it was pointed out that there exist significant modeling errors in the mathematical models of PVI's [2,3]. Faced with these modeling errors, we have two choices for the design of control: to make the model as accurate as possible—often with complexity—and to design a model-based control; or to design a robust control that employs minimal model knowledge and yet guarantees a performance level, while compensating for the error due to the model simplification. The former choice is likely to cost substantial time and effort for modeling, and to result in a control design imbedded with the model complexity. The latter approach, if there exists any feasible solution, deserves a serious consideration, which has been taken in our research.

As such a robust control technique, TDC is a strong candidate in that it has consistently shown in various applications its robustness against uncertainty such as modeling error, parameter variation, and disturbances [13–19]. Essential to the effectiveness of TDC is the contribution of the time delay estimation (TDE), a very effective and efficient estimation scheme of all the uncertainty by using the information at the previous time. While eliminating the uncertainty with the TDE, TDC introduces a desired closed-loop dynamics. Owing to the effectiveness and efficiency of the TDE, TDC has achieved performance levels as high as many other competent control laws.

For this reason, we have selected TDC as the active control and designed a TDC based on the new state space model. The design was experimented for the verification of its capability of simultaneous suppression with an accelerometer only.

This paper is organized as the following: Section 2 presents the derivation procedure and the result of the new state space model. Based on this new model, a TDC is designed and some remarks are made associated with its implementation in Section 3. Section 4 offers the procedure and results of experiments to verify the performance of the PVI controlled by TDC. In Section 5, the conclusion is drawn.

2. The new state space model of the PVI

Since a single chamber pneumatic spring is the simplest of all types of PVI's and serves as a basis for them, we have considered a single DOF PVI system consisting of a single chamber pneumatic spring and a payload, the schematic diagram of which is shown in Fig. 1.

As was explained in the introduction, the new state space model is desired to meet the requirement that the active control based on it is capable of simultaneous suppression with an accelerometer only. To this end, we first make a review of the physical model before deriving the new state space model.

2.1. The physical model of one DOF single chamber PVI [3]

As is illustrated in Fig. 1, the one DOF Single Chamber PVI consists of the payload, a diaphragm, and an air chamber. The physical model of the PVI has been derived from the equation of motion for the piston by using Newton's second law and the enthalpy equation for the chamber [3].[2] The resulting model was nonlinear, which was then linearized around nominal operating conditions to a set of linear equations as follows:

$$m_p \delta \dot{v}_p = A_p \cdot \delta P_t + F_d + E_{\text{diaphragm}} \tag{1}$$

[2] The derivation in [3] was made primary for a double (or dual) chamber case. Following the method in [3], one can easily carry out a modification to a single chamber case.

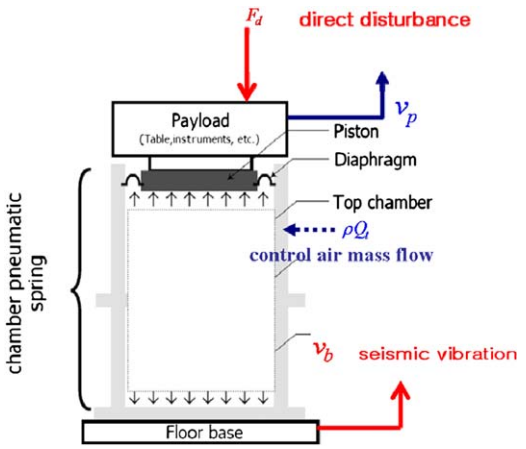

Fig. 1. Single DOF pneumatic vibration isolation system.

Table 2
Parameters of pneumatic spring and payload.

Symbol	Name	Value	
m_p	Payload	87	(kg)
ρ	Density	5.97	(kg/m^3)
R	Gas constant	286.9	(J/(kg K))
n	Specific heat ratio	1.4	
T	Temperature	288.1	(K)
P_0	Static pressure	3.51×10^5	(Pa)
V_t	Chamber volume	2.978×10^{-4}	(m^3)
A_P	Effective piston area	2.518×10^{-3}	(m^2)

and

$$\delta\dot{P}_t = -\frac{nA_pP_0}{V_t}\delta v_p + \frac{nRT}{V_t}\rho Q_t + \frac{nA_pP_0}{V_t}\delta v_b, \tag{2}$$

where m_p denotes the mass of the payload; δv_p the velocity of the payload; A_p the effective area of the payload to represent both cross-sectional area of the piston and movement of the diaphragm; δP_t the pressure of the chamber; F_d the direct disturbance; $E_{\text{diaphragm}}$ the modeling error due to the un-modeled diaphragm dynamics; ρQ_t the air mass-flow of control servo valve entering the chamber as the control input; δv_b the seismic vibration. The parameter values are listed for the pneumatic spring and the payload in Table 2.

Notice in (1) that the diaphragm dynamics is un-modeled deliberately and regarded as a modeling error ($E_{\text{diaphragm}}$) to be handled by a robust control. The diaphragm dynamics, which has been widely recognized as being complicated and difficult to model, has considerable impact on the discrepancy between the response predicted by the physical model and the experimental response [2,3].

In addition to the un-modeled diaphragm dynamics, there exist modeling errors due to the linearization of the original nonlinear model, due to inaccurate parameter values in (1) and (2), and due to the their variation as the system changes from one state to another. In short, (1) and (2) contain significant modeling errors described thus far.

2.2. New state space model of the PVI

In the physical model, (1) and (2), the control input is the air mass-flow, ρQ_t, to the chamber of the PVI. An inspection of (1) and (2) reveals that δv_b is directly affected by ρQ_t, but $E_{\text{diaphragm}}$ and F_d are not. In other words, the control input is not able to achieve simultaneous suppression, nor has any direct effect on the modeling error.

In order to obtain a new state space model that enables simultaneous suppression and direct control over the modeling error, we have applied the input–output linearization to the physical model. The input–output linearization performs successive differentiation of the system output until a derivative is directly related to the control input [11,12].

As the output of the PVI, we have selected the velocity of payload, δv_p, as follows:

$$v = \delta v_p. \tag{3}$$

Differentiating (3) w.r.t. time and rearranging (1), we obtain the time derivative of v as

$$\dot{v} = \delta \dot{v}_p = \frac{A_p}{m_p}\delta P_t + \frac{1}{m_p}(F_d + E_{\text{diaphragm}}). \tag{4}$$

Since (4) does not contain the control input, $\rho Q_t(t)$, on its right-hand-side, we need to differentiate (4) again as follows:

$$\ddot{v} = \delta \ddot{v}_p = \frac{A_p}{m_p}\delta \dot{P}_t + \frac{1}{m_p}(\dot{F}_d + \dot{E}_{\text{diaphragm}}). \tag{5}$$

Substituting (2) into (5), we obtain the following

$$\ddot{v} = -\frac{A_p}{m_p}\frac{nA_pP_0}{V_t}v + \frac{A_p}{m_p}\frac{nRT}{V_t}\rho Q_t(t) + \frac{1}{m_p}\left(\frac{nA_P^2P_0}{V_t}\delta v_b + \dot{F}_d + \dot{E}_{\text{diaphragm}}\right), \tag{6}$$

which now contains $\rho Q_t(t)$. Consequently, two successive differentiations v of have led to (6), which directly relates $\rho Q_t(t)$ to a derivative of v. The relative degree[3] of the PVI is two. Equation (6) may readily be expressed as a state equation, the new state space model we propose, as the following

$$\begin{bmatrix}\dot{v}\\ \ddot{v}\end{bmatrix} = \begin{bmatrix}0 & 1\\ -\frac{A_p}{m_p}\frac{nA_pP_0}{V_t} & 0\end{bmatrix}\begin{bmatrix}v\\ \dot{v}\end{bmatrix} + \begin{bmatrix}0\\ \frac{A_p}{m_p}\frac{nRT}{V_t}\end{bmatrix}\rho Q_t(t) + \begin{bmatrix}0\\ d_{\text{total}}\left\{ = \frac{1}{m_p}\left(\frac{nA_P^2P_0}{V_t}\delta v_b + \dot{F}_d + \dot{E}_{\text{diaphragm}}\right)\right\}\end{bmatrix}, \tag{7}$$

where d_{total} represents the uncertainties consisting of seismic vibration, direct disturbance, and the modeling error due to the diaphragm dynamics.

Note that the new state space model (7) is of the phase variable form (or the controllability canonical form). As a result, the model makes it possible for the control input ρQ_t to affect both seismic vibration and direct disturbance. To be more precise, however, ρQ_t affects $\dot{F}_d$ instead of F_d as shown in (7), and thus direct disturbance is affected only through the integration of ρQ_t.

It is also noteworthy that, in the new state space model, v and $\dot{v}$—velocity and acceleration—are used as its states, which are made available for feedback by employing an accelerometer and a numerical integration. In other words, an accelerometer suffices for state feedback. Besides, the control input of the new state space model is the air mass-flow, the same as the input of the physical model. Thus, the active control is to be performed in the flow control mode.

3. Time delay control design

TDC is a control technique which compensates for unpredicted disturbances with TDE [13–19]. Thanks to the effectiveness and the efficiency of TDE, TDC has a distinct robustness against disturbances, with a simpler structure and better efficiency than most of other advanced control algorithms developed until now. For this reason, we have made a decision to employ TDC for the active control. The detail of a TDC design is presented based on the new state space model of the PVI, along with several issues associated with its implementation.

Since TDC is designed to determine the control input of (7), $\rho Q_t(t)$, the active control with TDC, too, is supposed to share the same advantages mentioned in Section 2: simultaneous suppression and the use of an accelerometer only.

3.1. Derivation of TDC law

The new state space model (7) can be rewritten as

$$\rho Q_t(t) = \left(\frac{A_p}{m_p}\frac{nRT}{V_t}\right)^{-1}\ddot{v} + \left(\frac{A_p}{m_p}\frac{nRT}{V_t}\right)^{-1}\frac{A_p}{m_p}\frac{nA_pP_0}{V_t}v - \left(\frac{A_p}{m_p}\frac{nRT}{V_t}\right)^{-1}d_{\text{total}}, \tag{8}$$

which is rendered to a simple form as the following

$$\rho Q_t(t) = M\ddot{v} + V(v) + D_{\text{total}}, \tag{9}$$

where

$$M = \left(\frac{A_p}{m_p}\frac{nRT}{V_t}\right)^{-1}; \quad V(v) = M\frac{A_p}{m_p}\frac{nA_pP_0}{V_t}v; \quad D_{\text{total}} = -Md_{\text{total}}. \tag{10}$$

[3] A system is said to have *relative degree r*, if it is necessary to differentiate the output of a system r times to generate an explicit relationship between the output and input of the system.

Introducing a well-known positive constant, $\overline{M}$, we may express (9) as

$$\rho Q_t = \overline{M}\ddot{v} + (M-\overline{M})\ddot{v} + V(v) + D_{\text{total}}, \tag{11}$$

which results in an equivalent but different form as follows:

$$\rho Q_t = \overline{M}\ddot{v} + H(v,\ddot{v}), \tag{12}$$

where

$$H(v,\ddot{v}) = (M-\overline{M})\ddot{v} + V(v) + D_{\text{total}}. \tag{13}$$

In (12), the dynamics is partitioned into two categories: the part that is well-known, $\overline{M}\ddot{v}$; and the part that is uncertain and difficult to identify, $H(v,\ddot{v})$. More specifically, $H(v,\ddot{v})$ as (13) represents the difference of the total dynamics subtracted by the $\overline{M}\ddot{v}$ and thus it may be regarded as *net uncertainties*.

In the presence of $H(v,\ddot{v})$, TDC aims to achieve, regardless of such uncertainties, a desired dynamics:

$$\ddot{v} + K_D\dot{v} + K_P v = 0. \tag{14}$$

Typically, K_D is assigned with $2\zeta\omega_n$, and K_P with ω_n^2, so that the desired dynamics may have a pre-specified set of damping ratio and natural frequency of ζ and ω_n, respectively. To this end, the control input is designed as

$$\rho Q_t = \overline{M}u + \hat{H}(v,\ddot{v}) \tag{15}$$

and

$$u = -K_D\dot{v} - K_P v, \tag{16}$$

where $\hat{H}(v,\ddot{v})$ denotes an estimate of $H(v,\ddot{v})$.

Under the assumption that $H(v,\ddot{v})$ is continuous or at least piecewise continuous and time delay L is sufficiently small, holds the following approximation:

$$H(v,\ddot{v})_{t-L} \approx H(v,\ddot{v}), \tag{17}$$

where $\bullet_{t-L}$ denotes the value of $\bullet$ at the delayed time $t-L$. This approximation leads to the so-called Time Delay Estimation (TDE) as follows:

$$\hat{H}(v,\ddot{v}) \equiv H(v,\ddot{v})_{t-L}, \tag{18}$$

which is the idea essential to TDC. Note that the smaller L becomes, the better becomes the TDE. Since TDC is usually implemented in a discrete form, the smallest L is the *sampling period*. The TDE, $H(v,\ddot{v})_{t-L}$, is obtained from (12) as

$$\hat{H}(v,\ddot{v}) = H(v,\ddot{v})_{t-L} = \rho Q_{t-L} - \overline{M}\ddot{v}_{t-L}, \tag{19}$$

where ρQ_{t-L} is the control input already computed and used at the previous sampling time and $\overline{M}\ddot{v}_{t-L}$ is made available by differentiating $\dot{v}_{t-L}$. Comparison of (13) with (19) displays the ease and efficiency of the TDE. Specifically, whereas (13) requires both the values of model parameters and the estimate of total disturbances in (10), (19) neither necessitates to estimate such model parameters, nor requires the identification of disturbances.

Substituting (16) and (19) into (15), we obtain the final form of TDC:

$$\rho Q_t = \underbrace{\rho Q_{t-L} - \overline{M}\ddot{v}_{t-L}}_{\text{TDE: to cancel out } H(y,\dot{y},\ddot{y})} + \underbrace{\overline{M}(-K_D\dot{v} - K_P v)}_{u\text{: to inject desired dynamics}}. \tag{20}$$

Note that the TDE, $\rho Q_{t-L} - \overline{M}\ddot{v}_{t-L}$, is used to estimate and cancel the net uncertainties in (13), whereas $\overline{M}(-K_D\dot{v} - K_P v)$ is used to achieve the desired dynamics in (14). As a result, TDC in (20) requires little knowledge of model parameters and possesses a simple structure and high computational efficiency—approximately as efficient as a PID control. TDC in conjunction with the PVI system has the structure illustrated in Fig. 2.

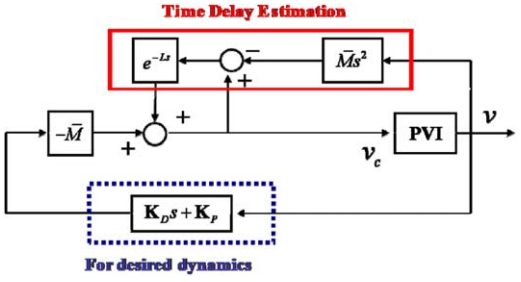

Fig. 2. Block diagram of PVI system controlled by TDC.

In (20), the selection of $\overline{M}$ is based on a stability condition. More specifically, $\overline{M}$ should be selected to meet the following condition [13–17]:

$$0 < \overline{M} \leq 2M, \tag{21}$$

where M as was defined in (9) is equal to $((A_p/m_p)(nRT/V_t))^{-1}$. A more detailed discussion on stability is presented in Appendix A. When the precise value of M is difficult to determine, it is tuned by trial and error. Further remarks will be made on its selection procedure in Section 3.2.

3.2. Practical issues on the design of TDC

3.2.1. 1st order approximation of control servo valve

The implementation of TDC in (20) requires the measurability of the air mass-flow $\rho Q_{t_{t-L}}$. Nevertheless, it was difficult to find an air mass-flow sensor that has a sufficient bandwidth and accuracy under high pressure (>3.51 bar) [20]. An alternative we have employed is a first-order approximation between the input (voltage, V_c) of the servo valve and the output (air mass-flow rate, ρQ_t) [10]:

$$\rho Q_t(s) = \frac{K}{\tau s + 1} V_c(s), \tag{22}$$

where τ denotes the time constant of the servo valve, and K stands for its flow gain.

Substituting (22) into (20), we have obtained a modified version of TDC as follows:

$$V'_c = \underbrace{V'_{c_{t-L}} - \overline{M}'\ddot{v}_{t-L}}_{\text{TDE: to cancel out } H(y,\dot{y},\ddot{y})} + \underbrace{\overline{M}'(-K_D\dot{v} - K_P v)}_{u\text{: to inject desired dynamics}}, \tag{23}$$

where $V'_c = L^{-1}\{(1/\tau s+1)V_c(s)\}$ and $\overline{M}' = \overline{M}/K$. V'_c in (23) requires the availability of v, $\dot{v}$ and $\ddot{v}$ for its implementation. Given the acceleration signal, $\dot{v}$, measured with an accelerometer, v is made available by the integration of the acceleration $\dot{v}$ w.r.t. time, whereas $\ddot{v}$ is obtained by the numerical differentiation of $\dot{v}$ with the *backward difference*. Therefore, V'_c in (23) is implementable with an accelerometer, only. The numerical differentiation, however, amplifies the noise in the acceleration signal, and requires a low-pass filter to attenuate the noise effect. The implementation of a filter will be mentioned in this subsection. Fig. 3 illustrates the block diagram of the PVI system controlled by TDC with the 1st order approximation of control servo valve.

3.2.2. Design procedure of the TDC

In order to implement TDC in (23), one needs to determine the gains ($\overline{M}'$, K_D and K_P) and the sampling time L. The selection of these constitutes the design procedure of TDC detailed as the following.

Step 1. Selection of L

It was pointed out in Section 3.1 that the smaller L provides the better performance, and that the smallest L available is the sampling time in a discrete system. Hence it is a rule of thumb to select L to be equal to the sampling time, which depends on the speed of the control hardware.

Step 2. Selection of K_D and K_P

K_D and K_P, first introduced in (14), are determined by the desired dynamics. For instance, a desired dynamics specified in terms of a natural frequency ω_n and a damping ratio ζ automatically determines K_D and K_P: $K_D = 2\zeta\omega_n$ and $K_P = \omega_n^2$, respectively.

Step 3. Selection of $\overline{M}'$

$\overline{M}'$ is chosen either by analytical relationships in (10) and (23) or by tuning—adjusting by trial and error. When there are the accurate values of parameters available, the former is preferable; or else, the latter approach is the more convenient.

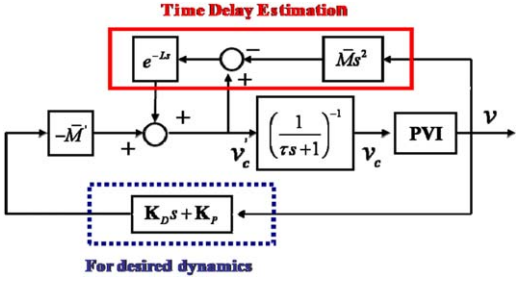

Fig. 3. Block diagram of PVI system controlled by TDC with the 1st order approximation of control servo valve.

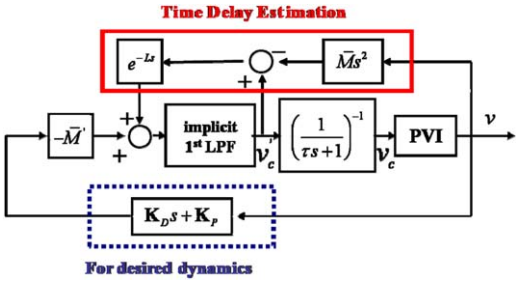

Fig. 4. Block diagram of PVI system controlled by TDC with the 1st order approximation of control servo valve and the implicit 1st digital low-pass filter (LPF).

In the selection of $\overline{M}'$, it is important to mention that lowering its value has the effect of using a 1st order low-pass filter [15,17]. In other words, by lowering $\overline{M}'$ it is possible to attenuate noise coming from the accelerometer [21], without explicitly using an additional low-pass filter shown in Fig. 4. The above considerations, therefore, offer two directions: Determine $\overline{M}'$ analytically and reduce it until noisy response vanishes in the closed-loop system behavior; or, set $\overline{M}'$ to have a small initial value, and then increase it by trial and error before the system begins to show noisy response.

Of the four parameters, L, K_D and K_P are determined straightforwardly; $\overline{M}'$ is the only gain that may have to be determined by trial and error. The selection procedure of these is significantly simpler than other control laws such as PID controls.

To summarize Section 3, we have derived TDC for the PVI from the new state space model, with the intended advantage of simultaneous suppression by using only an accelerometer. In addition to the advantage, TDC requires neither parameter values of the model, nor the estimate of the net uncertainties. Moreover, TDC has a simple gain selection procedure.

4. Experimental verification

Through the experiments, we are going to verify the claimed advantages of the TDC based on the new state space model: simultaneous suppression with an accelerometer; and the robustness and simplicity of TDC.

4.1. Experimental setup

As was introduced in Section 2, we have experimented on a single DOF PVI system consisting of a single chamber, a rubber diaphragm and a piston that supports a payload, as shown in Fig. 5. The payload weighs 85 kg, about one fourth of the payload of commercial pneumatics isolation tables supported by four pneumatic springs. To prevent tilting of the payload, the setup has been designed so that its mass center is located at a lower position—see Fig. 5.

The control system, based on dSPACE(ds1103) and Simulink of MATLAB(PC), takes sensor signals through A/D conversion, computes the control input, and transmits the input in the form of analog voltage to the control servo valve. The control servo valve, a proportional valve of nozzle-flapper type (Moog J814-0005, time constant: $\tau = 0.005$ s, flow gain: $K = 0.0001$ kg/s at 3.51 bar, 288.1 K), produces air mass-flow in proportion to the voltage from the control system, while keeping the static pressure to 3.51 bar in the single chamber.

We have tried to make the distance as short as possible between the control servo valve and the single chamber, as Fig. 5 shows. In order to measure the respective acceleration of the ground and the payload, we have attached to each of the ground and the payload a highly sensitive seismic accelerometer (PCB 393B31 with a sensitivity of 10 V/g). The accelerometer used in our experiment is Model 393B31 (PCB PIEZOTRONICS Co.), which was also shown to have sufficient reliability [5,6] and high sensitivity from 0.1 to 200 Hz [5,6,22]. Of these two accelerometers, only the latter is used for the PVI with TDC. Except for the accelerometer, we have not used other sensors at all. Fig. 6 shows the schematic diagram of the closed-loop system.

In accordance with the design procedure described in Section 3.2, we have selected gains as the following: L was set to be 0.001 s, the fastest sampling period the control system could achieve. Considering the normal practice of selecting the sampling frequency as 4–5 times that of the desired control bandwidth, one may regard the desired control bandwidth as 200–250 Hz, which is approximately equal to the actuator bandwidth, 200 Hz.

The desired dynamics was defined in terms of a damping ratio—critical damping—and a natural frequency as follows:

$$\zeta = 1, \quad \omega_n = 22\,\text{Hz}. \tag{24}$$

Hence, the desired dynamics explicitly specifies *no resonance peak* in the resulting closed-loop dynamics.

The selection of 22 Hz is out of the following considerations: Since the desired dynamics (14) is of a second order, the larger ω_n becomes, the smaller gets the transmissibility and the faster converges the response to direct disturbance. The highest possible frequency, according to [5], is 22 Hz that has the high coherence between the acceleration signal of the

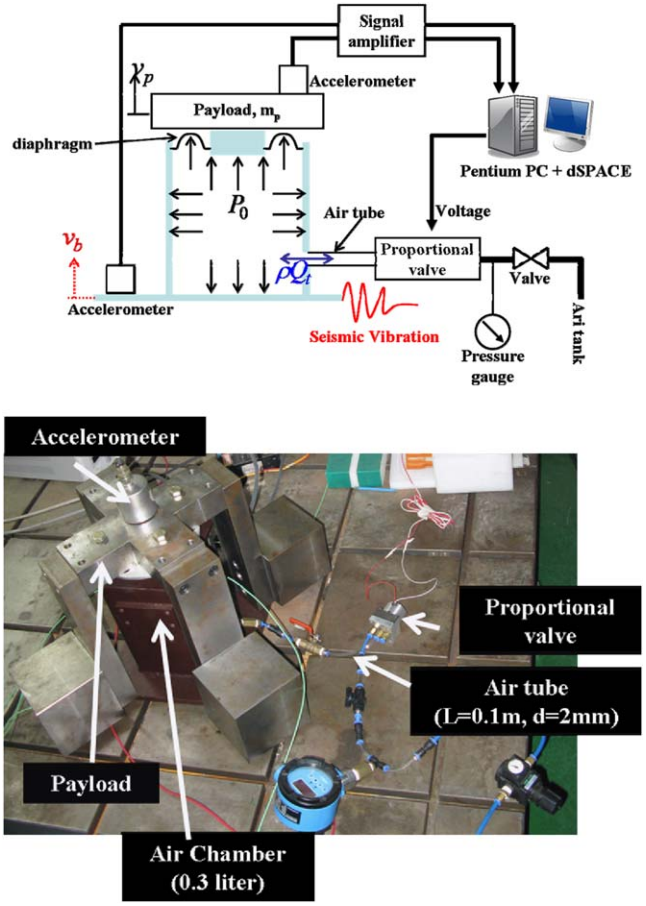

Fig. 5. Schematic diagram of actively controlled pneumatic vibration isolator system.

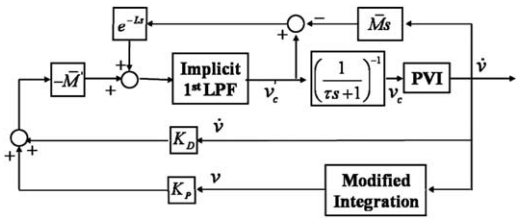

Fig. 6. Block diagram of pneumatic vibration isolator controlled by TDC, where v denotes the velocity of the payload.

payload and that of the ground. From (24), K_D and K_P are determined accordingly. $\overline{M}'$ was selected by the gain tuning procedure in the Step 3 of Section 3.2, which is

$$\overline{M}' = 0.04. \tag{25}$$

The ideal integration of the acceleration signal accompanies the accumulation of its DC bias [23], which causes the instability of the closed-loop system. A modified integration [24] is used, instead, as shown below

$$\frac{1}{s} \rightarrow \frac{1}{s+a}. \tag{26}$$

The parameter, a, affects the phase distortion of the signal as well as the extent of accumulation of the DC offset. As the value of a, 0.1 Hz was selected, based on the lower limit of the accelerometer, 0.1 Hz [22].

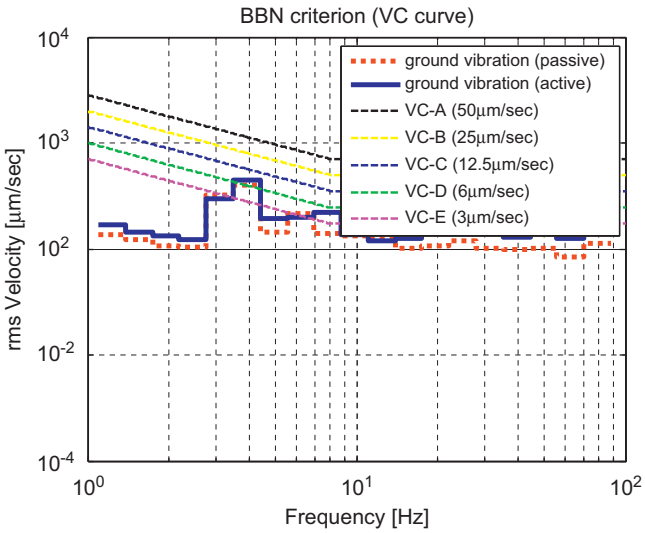

Fig. 7. The 1/3 octave band analysis results for seismic vibration of passive (not controlled) and actively controlled PVI system: ▪▪▪▪ red dotted line, passive one; ▬ blue solid line, active one. (For interpretation of the references to color in this figure legend, the reader is referred to the web version of this article.)

4.2. Experimental result

Experiments have been carried out to test the performance of the PVI controlled by TDC for three cases: (1) under seismic vibration; (2) under direct disturbance; and (3) under both seismic vibration and direct disturbance.

4.2.1. Suppression of seismic vibration

In order to observe the suppression performance of seismic vibration, the transmissibility between the base and the payload is estimated as follows:

$$\text{transmissibility} = \frac{G_{SP}}{G_{SS}}, \tag{27}$$

where the subscripts '*S*' and '*P*' stand for the acceleration signal of seismic vibration and that of the payload, respectively; G_{SS} denotes auto-power spectral density function, and G_{SP} cross-power spectral density function. The transmissibility was estimated by applying Hanning window under the ensemble average of 50 times, and observed with the frequency resolution of 0.2 Hz.

Fig. 7 shows the spectra of the two seismic vibrations—a passive one and an active one—in comparison with the BBN vibration criteria. Both the passive vibration and the active vibration represent the vibration generated by a male adult with the weight of about 70 kg jumping near the PVI. Fig. 7 shows the spectra of the two vibrations, obtained by 1/3 octave band analysis, where the passive and active seismic vibration reaches approximately the level of the VC-C.

Fig. 8 shows the respective transmissibility due to the passive isolator and the PVI controlled by TDC between the base and the payload, in a linear scale and a logarithmic scale, respectively. The transmissibility due to the PVI controlled by the TDC shows virtually no resonance peak in the low frequency range: it has the maximum peak of 0.1932 whereas that of the passive isolator reaches 9.8406 at its resonance. Recalling that no resonance peak was desired and specified by setting $\zeta = 1$ in the desired dynamics, one confirms its realization here. Incidentally, the result is far better than the already impressive result reported in [5], where the maximum peak achieved was about 1/20 of that of the passive isolator.

From Fig. 8, the root mean square (RMS) values about the magnitude of transmissibility are listed in Table 3. As shown in Table 3, TDC substantially suppresses seismic vibration in low frequency range, especially from 1 to 10 Hz. However, the suppression performance due to TDC becomes slightly worse than that of the passive PVI between 10 and 30 Hz. This degradation results from the fundamental design limitation associated with the desired dynamics, which is a 2nd order linear dynamics ($\zeta = 1$ and $\omega_n = 22$ Hz). If a better suppression is desired between 10 and 30 Hz, ω_n should be reduced at the risk of degrading transient response due to direct disturbance.

Fig. 9 shows the *time response* of the payload acceleration resulted from seismic vibration, which too demonstrates the effectiveness of the PVI with TDC.

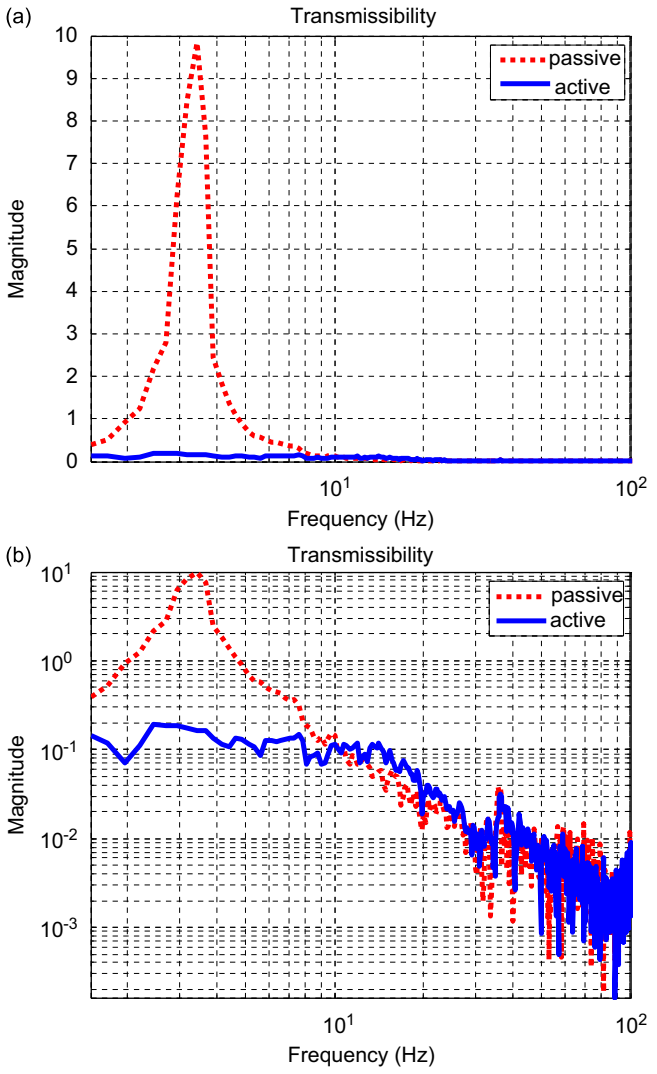

Fig. 8. (Seismic vibration) transmissibility of passive isolator and the PVI Controlled by the TDC: (a) Linear scale; (b) Log scale; red dotted line, passive one; blue solid line, TDC. (For interpretation of the references to color in this figure legend, the reader is referred to the web version of this article.)

Table 3
RMS value of transmissibility's magnitude from Fig. 8.

		Passive	TDC
Root means square (RMS)	1–10 Hz	2.8345	0.1291
	10–30 Hz	0.0445	0.0618

4.2.2. Suppression of direct disturbance

Direct disturbance was generated with an impact by a rubber hammer to the payload. Under this disturbance, we have compared its suppression by TDC with that by the passive isolator in terms of the settling time of the payload.

Fig. 10 shows the time response of the payload resulted from direct disturbance. In Fig. 10(a) the 2 percent settling time[4] was about 3.10 s with the passive isolator, whereas in Fig. 10(b) it was 0.99 s with TDC—a 68 percent reduction in the settling time with the latter. This performance is approximately of the same level as that reported in [7].

[4] The 2 percent *settling time* is the time required for the response to reach and stay within 2 percent of the final value.

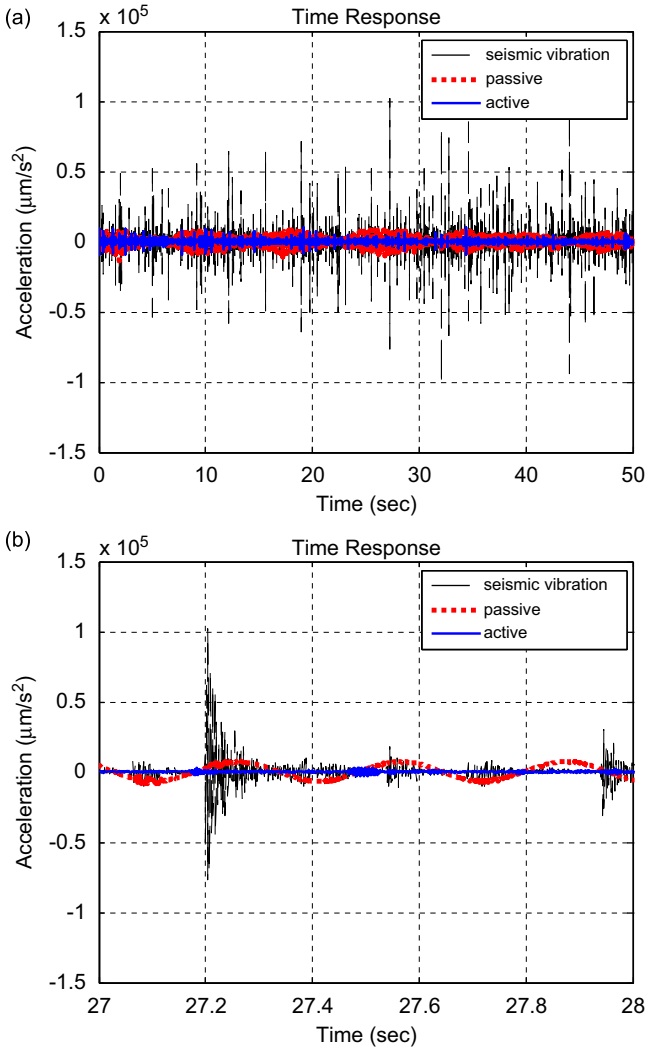

Fig. 9. (Seismic vibration) time domain response of the payload in passive isolator and the PVI controlled by the TDC: (a) 0–50 s; (b) 27–28 s; — · — black dashed line, seismic vibration; red dotted line, passive one; blue solid line, TDC. (For interpretation of the references to color in this figure legend, the reader is referred to the web version of this article.)

Fig. 11 shows the power spectral density (PSD) plot obtained from Fig. 10. We confirm that, although there was the limit to suppress high-frequency part of F_d due to the effect of integration as introduced in Section 2, TDC substantially suppresses direct disturbance in low frequency range, especially from 1 to 10 Hz. Because direct disturbance in the low frequency range is substantially suppressed by TDC, the settling time of the payload resulted from direct disturbance in the PVI with TDC is significantly shorter than the case of passive PVI as shown in Fig. 10. Clearly, the PVI with TDC is effective in the suppression of direct disturbance.

4.2.3. Simultaneous suppression of seismic vibration and direct disturbance

Simultaneous suppression was experimented with seismic vibration and direct disturbance being applied simultaneously. Each of the two disturbances was generated in the same way as before, but this time together at the same time.

Fig. 12 shows the time response of the payload resulting from seismic vibration and direct disturbance. The settling time of the PVI with TDC is significantly less than that of the passive PVI. In addition, resonance is observed in the steady-state response of the latter, which is hardly observed in that of the former. The result makes it evident that the PVI with TDC is effective in simultaneous suppression.

The experiments for the three cases so far have verified that the PVI with TDC is effective in suppressing each and both of seismic vibration and direct disturbance—this effectiveness has been achieved with an accelerometer only. How the disturbances were suppressed in the presence of *modeling error* deserves a final analysis. More specifically, we want to

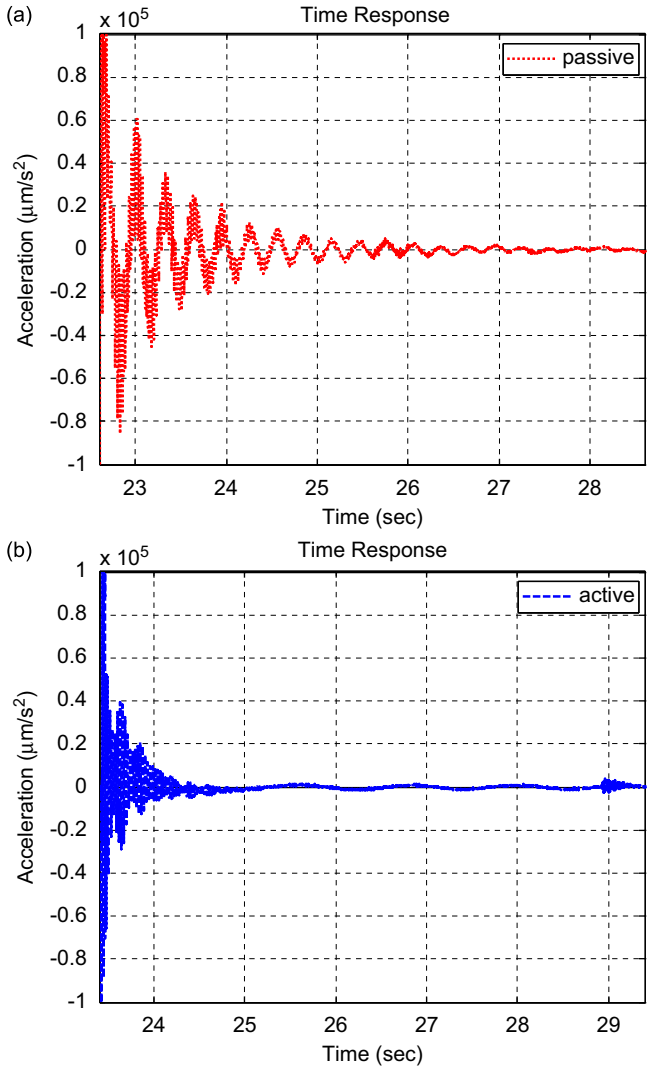

Fig. 10. (Direct disturbance) time domain response of the payload in passive isolator and the PVI controlled by the TDC: (a) passive one (▪▪▪▪ red dotted line); (b) TDC (▬ blue solid line). (For interpretation of the references to color in this figure legend, the reader is referred to the web version of this article.)

discuss on how accurately TDC could estimate and eliminate $H(v,\ddot{v})$ in (13), the net uncertainties, which is the collection of all disturbances and modeling errors.

4.3. Analysis and discussions

As was described, TDC employs the TDE to estimate and eliminate the net uncertainties $H(v,\ddot{v})$—let it be denoted by H for the sake of notational convenience. The accuracy of the TDE is directly related to the achievement of the desired dynamics, since substituting (22) and (23) into (12) leads to the following dynamics:

$$\ddot{v}+K_D\dot{v}+K_P v=\overline{M}^{-1}(\hat{H}-H). \tag{28}$$

Hence, the smaller is $H-\hat{H}$, which is the TDE error, the closer converges the closed-loop dynamics to the desired dynamics (14). Insomuch as the TDE is accurate, TDC is effective in handling disturbances and modeling errors, thereby explaining the performance demonstrated by the experimental results above.

In an attempt to investigate the accuracy of the TDE, we are going to compare the estimated uncertainty ($\hat{H}$) with the real uncertainty (H). $\hat{H}$ can be obtained by virtue of (19); H, however, cannot be obtained from (13), but can only be obtained indirectly from (12) and (22) on the off-line basis. Hence,

$$\hat{H}=V_{c_{t-L}}-\overline{M}\ddot{v}_{t-L} \tag{29}$$

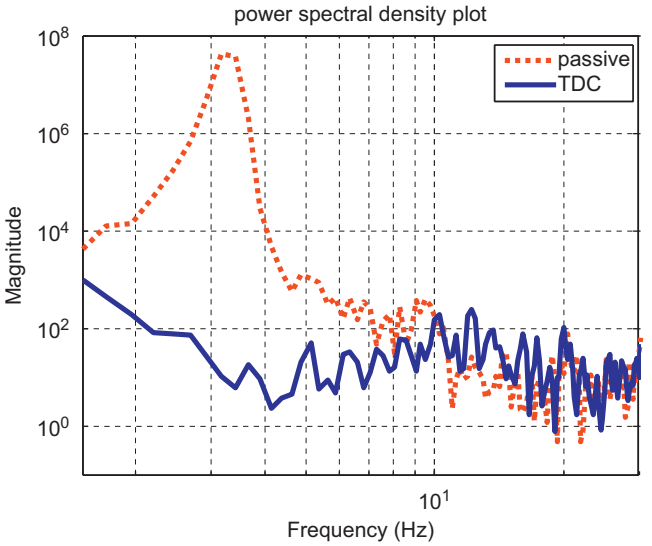

Fig. 11. (Direct disturbance) power spectral density plot resulted from Fig. 10: (a) passive one (red dotted line); (b) TDC (blue solid line). (For interpretation of the references to color in this figure legend, the reader is referred to the web version of this article.)

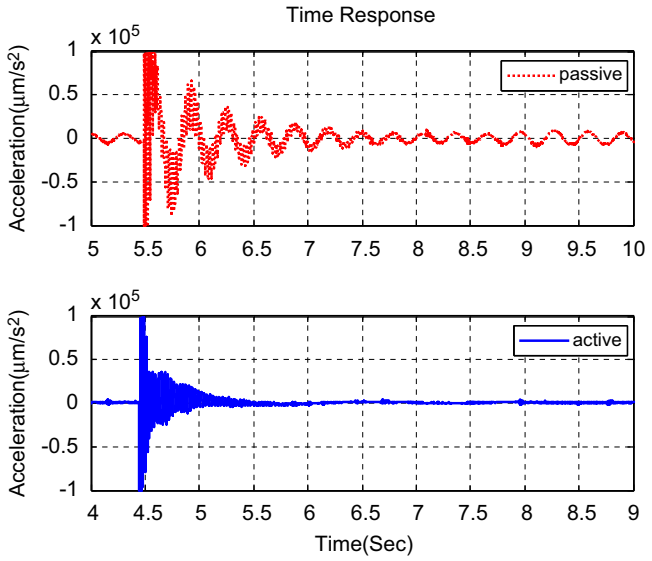

Fig. 12. (Seismic vibration+Direct disturbance) Time domain response of the payload in passive isolator and the PVI controlled by the TDC: passive one (red dotted line); TDC (blue solid line). (For interpretation of the references to color in this figure legend, the reader is referred to the web version of this article.)

and

$$H = V'_{c_t} - \overline{M}\ddot{v}_t. \tag{30}$$

$\hat{H}$ in (29) is made available *after* an experiment, simply by retrieving the data actually used—note in (23) that $\hat{H}$ was computed in real-time control—in the experiment. H in (30) is evaluated after an experiment, too. The difference, however, is that the jerk signal $\ddot{v}(t)$ is calculated by an off-line numerical scheme [25] to differentiate the signal from the accelerometer. This numerical differentiation scheme is highly sophisticated and much more accurate than the backward difference scheme employed in (23) to calculate $\ddot{v}_{t-L}$ on real-time basis. In the absence of an appropriate sensor for the jerk signal, the above approach is perhaps the best alternative to evaluate H.

Fig. 13(a) displays both H and $H-\hat{H}$ in the case that the PVI with TDC is subject to seismic vibration, only. In this case, the experimental result shows that $H_{\text{rms}} = 1.13 \times 10^{-2}$ V whereas $(H-\hat{H})_{\text{rms}} = 3.53 \times 10^{-4}$ V, where $(\bullet)_{\text{rms}}$ denotes the root-mean-square of $(\bullet)$. Hence, the accuracy of the TDE is of less than 3.12 percent rms error, enabling to estimate and

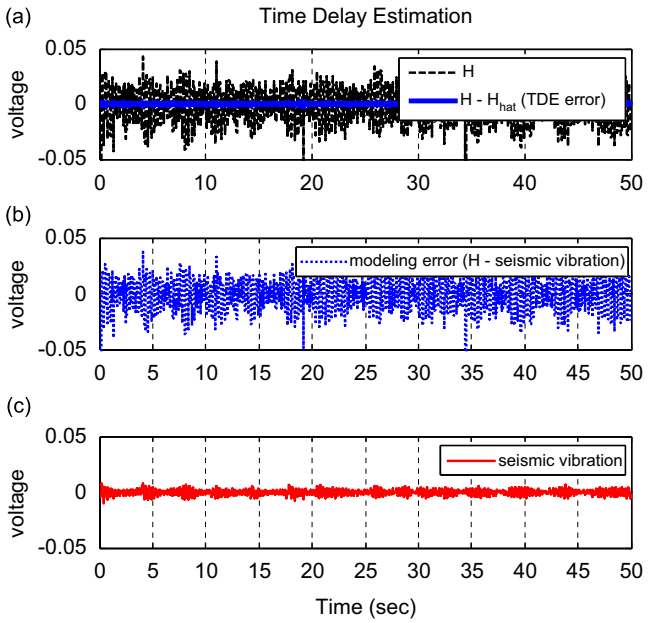

Fig. 13. (Seismic vibration) TDE in the PVI controlled by the TDC: (a) H (– – – black dashed line) and $H-\hat{H}$ (blue solid line); (b) $H-d_{\text{seismic}}$ (blue dotted line); (c) d_{seismic} (red solid line). (For interpretation of the references to color in this figure legend, the reader is referred to the web version of this article.)

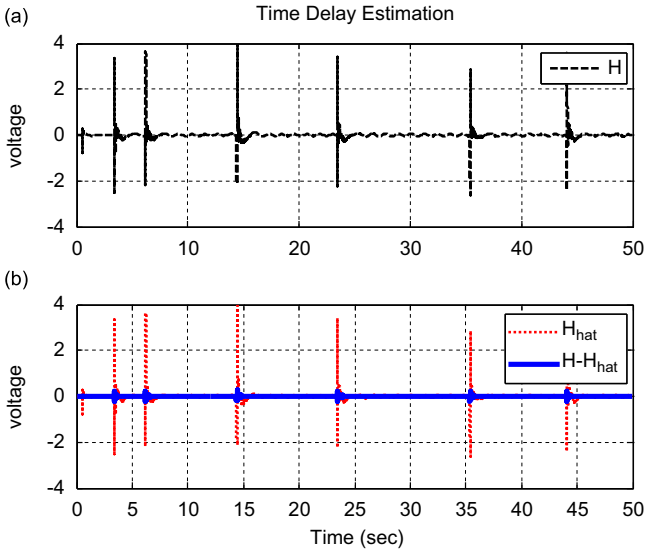

Fig. 14. (Direct disturbance) TDE in the PVI controlled by the TDC: (a) H (– – – black dashed line); (b) $\hat{H}$ (red dotted line) and $H-\hat{H}$ (blue solid line). (For interpretation of the references to color in this figure legend, the reader is referred to the web version of this article.)

eliminate 96.88 percent of the total uncertainty, thereby accounting for the performance level observed in the experimental results.

Whereas Fig. 13(a) shows the total uncertainty H, Figs. 13(b) and (c) shows the *respective share* of its components: seismic vibration d_{seismic}, and the modeling error, $(H-d_{\text{seismic}})$—See (13). Here d_{seismic} was obtained by combining (8), (9), (13) and (35) as

$$d_{\text{seismic}} = -\frac{M}{Km_p}\,\frac{nA_p^2P_0}{V_t}\,\delta v_b, \tag{31}$$

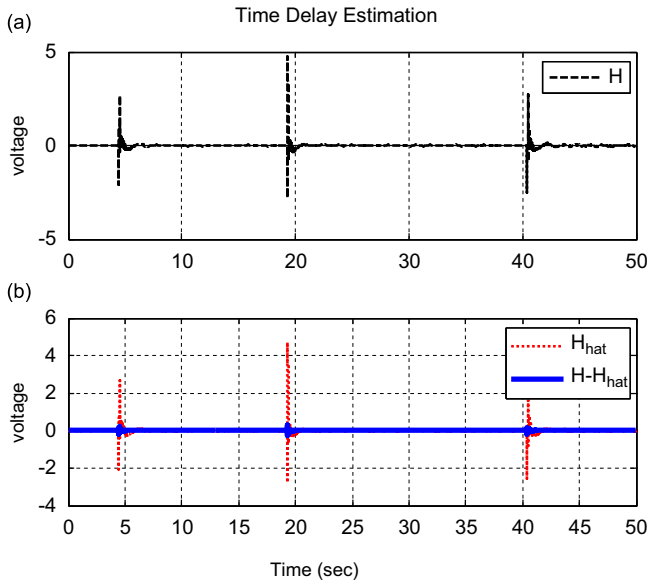

Fig. 15. (Seismic vibration+Direct disturbance) TDE in the PVI controlled by the TDC: (a) H (– – – black dashed line); (b) $\hat{H}$ (▪▪▪▪▪ red dotted line) and $H-\hat{H}$ (▬▬ blue solid line). (For interpretation of the references to color in this figure legend, the reader is referred to the web version of this article.)

where δv_b is obtained by integrating the acceleration signal. Of the two, the share due to the modeling error is far larger than that of seismic vibration. The predominance of the former makes it clear that a good active control should be able to handle the modeling error, and that the PVI with TDC is competent to do so.

Fig. 14 displays H, $\hat{H}$ and $H-\hat{H}$ when direct disturbance is being applied, where the spikes represent the impacts produced by the hammer. Note that both Fig. 10 and Fig. 14 come from the same experiment; the former closes up the time response within the time span between 23.5 s and 29.5 s. Fig. 14(b) shows that the TDE remains accurate—$(H-\hat{H})_{\mathrm{rms}}/H_{\mathrm{rms}}=0.050$—even under direct disturbance, which is sharp and discontinuous, explaining the performance observed in Fig. 10. Incidentally, owing to the difficulty of evaluating F_d, we were unable to identify the respective portion of the modeling error and direct disturbance.

In the case of simultaneous suppression, too, one can obtain the same level of accuracy in the TDE—$(H-\hat{H})_{\mathrm{rms}}/H_{\mathrm{rms}}=0.047$—shown in Fig. 15(b), which accounts for the performance in Fig. 12.

5. Conclusion

Out of the discussion on the MSD model and the physical model, we have taken a third direction for a new state space representation, which has been proposed in this article. Owing to the new state space model, it has become possible for the control input to affect both seismic vibration and direct disturbance with an accelerometer only.

Based on this model, the TDC design has been carried out. Thanks to TDC, each and both of seismic vibration and direct disturbance have been suppressed effectively and efficiently in the presence of substantial modeling error.

A practical implication is that one may be able to greatly extend the lower limit of the frequency range where a resonance peak is nonexistent. For those who demand vibration isolation at such low frequency range, the PVI with TDC is a good candidate and worthy of consideration.

Acknowledgment

This work has been financially supported by Basic Research Program of Korea Science and Engineering Foundation (KOSEF) grant funded by the Korea government (MOST) (No. R01-2006-000-10872-0).

Appendix A. Stability analysis of TDC

In (20), the selection of $\overline{M}$ is based on a stability condition. That is, the selection of $\overline{M}$ is related with the robustness margin. In order to derive the stability condition of TDC, the closed-loop dynamics can be obtained by combining (8) and (20) as

$$\{[(1-e^{-Ls})+M^{-1}\overline{M}e^{-Ls}]s^2+[M^{-1}\overline{M}K_D]s+[(1-e^{-Ls})B+M^{-1}\overline{M}K_P]\}V(s)=(1-e^{-Ls})d_{\mathrm{total}}(s), \tag{32}$$

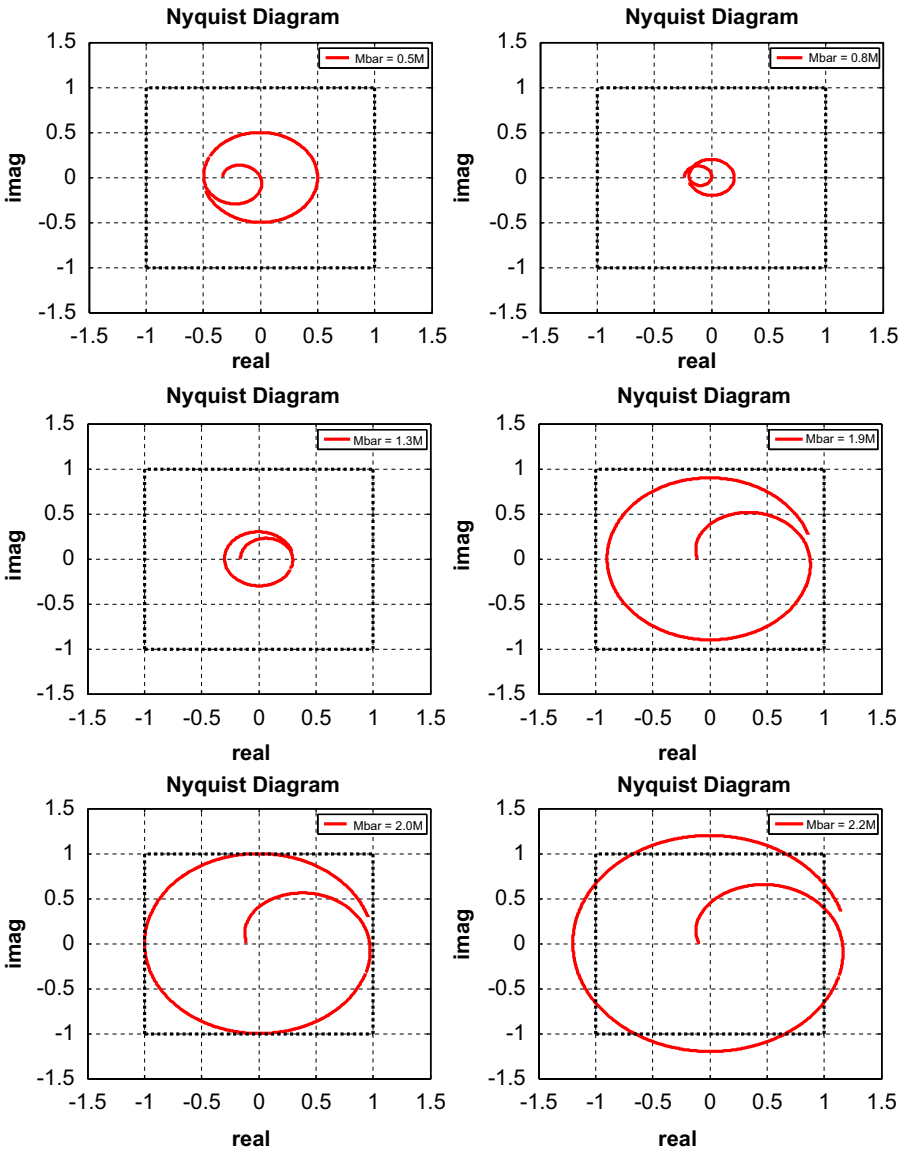

Fig. 16. Nyquist diagram for PVI system controlled by TDC.

where s denotes the Laplace operator; M as was defined in (9) is equal to $((A_p/m_p)(nRT/V_t))^{-1}$; B denotes $(A_p/m_p)(nA_pP_0/V_t)$; $V(s)=\mathbf{L}(v(t))$.

The characteristic equation is given by

$$\{[(1-e^{-Ls})+M^{-1}\overline{M}e^{-Ls}]s^2+[M^{-1}\overline{M}K_D]s+[(1-e^{-Ls})B+M^{-1}\overline{M}K_P]\}V(s)=0$$

$$\Rightarrow -[(1-M^{-1}\overline{M})s^2+B]e^{-Ls}+[s^2+M^{-1}\overline{M}K_Ds+(M^{-1}\overline{M}K_P+B)]=0 \Rightarrow 1-\frac{[(1-M^{-1}\overline{M})s^2+B]e^{-Ls}}{[s^2+M^{-1}\overline{M}K_Ds+(M^{-1}\overline{M}K_P+B)]}=0. \quad (33)$$

To determine whether the characteristic equation is stable or not, Nyquist criterion is employed for the transfer function,

$$g(s)=\frac{-[(1-M^{-1}\overline{M})s^2+B]e^{-Ls}}{[s^2+M^{-1}\overline{M}K_Ds+(M^{-1}\overline{M}K_P+B)]}, \quad s=j\omega. \quad (34)$$

As $\omega\to\infty$, the map of $g(j\omega)$ converges to a circle of radius $|(1-M^{-1}\overline{M})|$ [14]. The Nyquist diagrams of Fig. 16 are shown for $\overline{M}=0.5M$, $0.8M$, $1.3M$, $1.9M$, $2.0M$ and $2.2M$ with $\zeta=1$, $\omega_n=22$ (Hz). That is, the gain margin can be defined

as $-20\log|(1-M^{-1}\overline{M})|$(dB). For the Nyquist diagram not to enclose the -1 point, the gain margin should be positive. Therefore, $\overline{M}$ should be selected to meet the following condition [13–17]:

$$|(1-M^{-1}\overline{M})|<1, \text{ that is } 0<\overline{M}<2M. \tag{35}$$

Notice that as $\overline{M}\to M$, the gain margin is increasing.

References

[1] M. Heertjes, N. van de Wouw, Nonlinear dynamics and control of a pneumatic vibration isolator, *Journal of Vibration and Acoustics, Transactions of the ASME* 128 (4) (2006) 439–448.
[2] J.-H. Lee, K.-J. Kim, Modeling of nonlinear complex stiffness of dual-chamber pneumatic spring for precision vibration isolations, *Journal of Sound and Vibration* 301 (3–5) (2007) 909–926.
[3] C. Erin, B. Wilson, An improved model of the pneumatic vibration isolator: theory and experiment, *Journal of Sound and Vibration* 218 (1998) 81–101.
[4] C.G. Gordon, Generic vibration criteria for vibration-sensitive equipment, in: Proceedings of SPIE, San Jose, CA, 1999.
[5] Y.-H. Shin, K.-J. Kim, Performance enhancement of pneumatic vibration isolation tables in low frequency range by time delay control, *Journal of Sound and Vibration* 321 (3–5) (2009) 537–553.
[6] Y.-H. Shin, Performance enhancement in pneumatic vibration isolation tables at low frequencies by time delay control, Ph.D. Thesis, Department of Mechanical Engineering, Korea Advanced Institute of Science and Technology, February 2009.
[7] S.-H. An, H.-s. Kim, K.-H. Riim, Active control of vibration isolation table using air-spring, *Korea Society for Noise and Vibration Engineering* 17 (7) (2007) 565–571.
[8] K. Kawashima, T. Kato, K. Sawamoto, T. Kagawa, Realization of virtual sub chamber on active controlled pneumatic isolation table with pressure differentiator, *Precision Engineering* 31 (2007) 139–145.
[9] T. Kato, K. Kawashima, K. Sawamoto, T. Kagawa, Active control of a pneumatic isolation table using model following control and a pressure differentiator, *Precision Engineering* 31 (2007) 269–275.
[10] P.-C. Chen, M.-C. Shih, Modeling and robust active control of a pneumatic vibration isolator, *Journal of Vibration and Control* 13 (2007) 1553–1571.
[11] A. Isidori, *Nonlinear Control Systems: An Introduction, Lecture Notes in Control and Information Sciences*, second ed, Springer, Berlin, 1989.
[12] J.-J.E. Slotine, W. Li, *Applied Nonlinear Control*, Prentice-Hall, Englewood Cliffs, NJ, 1991.
[13] K. Youcef-Toumi, O. Ito, A time delay controller design for systems with unknown dynamics, *ASME Journal of Dynamic Systems, Measurement and Control* 112 (1990) 133–142.
[14] K. Youcef-Toumi, S. Reddy, Analysis of linear time invariant systems with time delay, *ASME Journal of Dynamic Systems, Measurement and Control* 114 (1992) 544–555.
[15] K. Youcef-Toumi, S.T. Wu, Input/output linearization using time delay control, *ASME Journal of Dynamic Systems, Measurement and Control* 114 (1992) 10–19.
[16] T.C. Hsia, A new technique for robust control of servo systems, *IEEE Transactions on Industrial Electronics* 36 (1989) 1–7.
[17] M. Jin, S.H. Kang, P.H. Chang, Robust compliant motion control of robot with nonlinear friction using time-delay estimation, *IEEE Transactions on Industrial Electronics* 55 (1) (2008) 258–269.
[18] P.H. Chang, J.H. Jung, A systematic method for gain selection of robust PID control for nonlinear plants of second-order controller canonical form, *IEEE Transactions on Control Systems Technology* 17 (2009) 473–483.
[19] M. Jin, P.H. Chang, Simple robust technique using time delay estimation for the control and synchronization of Lorenz systems, *Chaos, Solitons and Fractals* 41 (2009) 2672–2680.
[20] T. Funaki, K. Kawashima, T. Kagawa, Dynamic characteristic analysis of laminar flow meter, in: *SICE Annual Conference* in Fukui, 2003.
[21] F.A. Levinzon, Fundamental noise limit of piezoelectric accelerometer, *IEEE Sensors Journal* 4 (1) (2004) 108–111.
[22] 〈http://www.pcb.com/spec_sheet.asp?model=393B31〉.
[23] Y.K. Thong, M.S. Woolfson, J.A. Crowe, B.R. Hayes-Gill, R.E. Challis, Dependence of inertial measurements of distance on accelerometer noise, *Measurement Science & Technology* 13 (2002) 1163–1172.
[24] W.-H. Zhu, B. Tryggvason, J.-C. Piedboeuf, On active acceleration control of vibration isolation systems, *Control Engineering Practice* 14 (8) (2006) 863–873.
[25] A. Savitzky, M.J.E. Golay, Smoothing and differentiation of data by simplified least squares procedures, *Analytical Chemistry* 36 (1964) 1627–1639.